Towards Automatic Flight Control for Commercial Airliners in Formation Flight [*]

D. Büchner [*] **J.A.A. Engelbrecht** [*] **J. Adams** [**]
C. Redelinghuys [**]

[*] *Stellenbosch University, Stellenbosch, South Africa*
[**] *University of Cape Town, Cape Town, South Africa*

Abstract: This paper presents research done towards the goal of achieving automatic flight control for commercial airliners in formation flight. The motivation for this research is to ultimately reduce fuel-consumption through a reduction in the drag of the follower aircraft, which is a result of the formation flight. Traditional aerodynamic equations for conventional flight of fixed-wing aircraft are expanded to include formation flight interactions. A trim analysis uncovers risks, challenges and feasible trim regions for the formation follower to maintain. These regions include a potentially risky region which is sandwiched between two untrimmable regions, with respect to a maximum aileron setting, and an outside region which has only one untrimmable bound, making it less risky but with lower fuel-consumption benefit. Next, a state space representation is constructed, allowing for a linear dynamics analysis. The poles and their movement as a function of the lateral and vertical separation of the follower aircraft relative to the leader aircraft are shown, and indicate greater changes in flight dynamics due to vertical separation than to lateral separation. The results of the trim analysis and linear dynamics analysis form the basis for the design of a formation flight control system.

Keywords: Aircraft control, autonomous control, flight control, formation flight, linear analysis, non-linear models, stability analysis, state space models, trim analysis

NOMENCLATURE

a_1	Tailplane lift coefficient
AR	Aspect ratio
$b, \bar{c}$	Wingspan, wing chord
b_f	Double the tailfin height
b_h	Tailplane span
c_{l_α}	2-D wing lift coefficient gradient
C_D	Drag coefficient
C_L	Lift coefficient
C_l	Rolling moment coefficient
C_m	Pitching moment coefficient
C_n	Yawing moment coefficient
C_S	Sideforce coefficient in stability frame
C_Y	Sideforce coefficient in body frame
C_X	Longitudinal force in body frame
C_Z	Vertical force in body frame
g	Gravitational acceleration
h	Mass centre position
h_0	Wing aerodynamic centre
I_{xx}, I_{yy}, I_{zz}	Moments of inertia in body frame
m	Aircraft mass (unloaded aircraft)
M	Mach number
$\bar{q}$	Dynamic pressure ($\frac{1}{2}\rho\bar{V}^2$)
r_c	Core radius
S, S_f	Wing area, tailfin area
T	Thrust
u, v, w	Linear velocity components
p, q, r	Angular velocity components
$\overline{V}$	Freestream velocity
$\overline{V}_s$	Speed of sound in air
V_f, V_T	Tail volume ratio, fin volume ratio
α	Angle of attack
β	Sideslip angle
$\delta_a, \delta_e, \delta_r$	Aileron, elevator, rudder deflection angles
ϵ	Downwash angle
η	Lateral separation normalised to wingspan
ζ	Vertical separation normalised to wingspan
ζ_f	$\frac{b_f}{b}$
ζ_v	$\frac{z_v}{b}$
η_h	$\frac{b_h}{b}$
θ, ϕ, ψ	Pitch, roll and yaw angle
μ	$\frac{r_c}{b}$
ρ	Air density
σ	Downwash influence factor
τ	Moment influence factor

Subscripts

c	Conventional isolated flight
f	Tailfin
f'	Formation flight conditions
j	Lead aircraft
k	Follower aircraft
t	Trim flight conditions

1. INTRODUCTION

In the passenger air-travel industry, there is a growing demand for the reduction of fuel-consumption with en-

vironmental and cost benefits in mind. Formation flight allows for a decrease in induced drag and a reduction in fuel consumption. Wind-tunnel tests have shown that, depending on the formation flight configuration, drag reductions of as high as 25% may be achieved (Blake and Gingras 2004). An analysis by Bower et al. (2009) showed that, when formation geometries and route optimisation are considered for commercial airliners, a 13% reduction in fuel consumption may be realised.

A previous study performed by Bizinos and Redelinghuys (2012) investigated the aerodynamic interaction of aircraft flying in formation. An aerodynamic model was derived for the induced forces and moments experienced by a trailing aircraft due to the trailing vortices of the lead aircraft. It was found that a very non-linear relationship exists between these induced forces and moments and the separation between the two aircraft, and that the changes are particularly steep near the optimum separation distance.

The results of this study lead to questions about the stability and performance of the flight control system of the trailing aircraft in formation flight. The induced forces and moments would require unconventional trim settings for the trailing aircraft's control surfaces. For example, the ailerons would have a non-zero trim setting due to the constant rolling moment experienced by the trailing aircraft. Since the changes in the forces and moments are steep near the optimum separation distance, the trim settings would also be very sensitive to small changes in the position of the trailing aircraft relative to the leading aircraft.

Formation flight also has implications for the feedback control gains of the flight control system. The presence of the leading aircraft can be modelled as changes in the aerodynamic coefficients of the trailing aircraft, which manifest as changes in the aerodynamic stability and control derivatives on which the feedback gain calculations are based. The changes in the aerodynamic stability and control derivatives of the trailing aircraft due to the presence of the leading aircraft would therefore lead to reduced flight control performance and even instability. The flight control gains would therefore have to be redesigned and gain scheduled as a function of the separation distance.

The research presented in this paper is the initial steps towards investigating the implications of formation flight for the flight control systems of passenger airliners. The trim analysis and linearised dynamic model derived in this paper will serve as the basis for evaluating the stability and performance of current flight control systems in formation flight. Once the baseline has been established, the specialised requirements that formation flight place on the flight control system will be determined, and a new flight control architecture will be proposed, implemented and evaluated.

Previous research on flight control in formation flight include two papers by Brodecki et al.. Their research shows the design of a control system that addresses the unique environment encountered by an aircraft flying in formation in the upwash of the formation leader. The control system uses an advanced extremum seeking algorithm which utilises an EKF to estimate gradients, as the exact postion

of the sweet spot cannot practically be known (Brodecki et al. 2013a). Furthermore, the emergent behaviour of the control system is investigated. The desired echelon formation emerges consistently after formation is initialized at random points using a Monte Carlo scheme. This is achieved without inter-vehicle communication, using only minimal information about the other formation members and the extremum seeking algorithm, which drives each member to the sweet spot for fuel consumption minimisation (Brodecki et al. 2013b).

Studies, such as Zou et al. (2009), show a trend of interest in formation flight due to fuel consumption reductions, though complete formation flight interactions were not yet adequately modelled, or were not yet taken into account at this stage. The assumption was made that an uncertainty in the induced drag coefficient for formation followers exists, and an adaptation algorithm was developed to estimate the drag coefficient. A control algorithm was designed to achieve formation flight within an arbitrarily small bounded tracking error.

2. AERODYNAMIC INTERACTIONS AND TRIM SETTINGS

2.1 Induced Forces and Moments

A model for the induced forces and moments experienced by a trailing aircraft in formation flight was derived by Bizinos and Redelinghuys (2012). In this paper, the model is analysed to determine the required trim settings and dynamic response of the trailing aircraft as a function of lateral and vertical separation relative to the leading aircraft. The standard aerodynamic equations expressed in wind axes are expanded as shown in (1) with the formation flight effects included, denoted by subscript f'.

$$
\begin{aligned}
C_D ={}& C_{Dt,c} + C_{D_\alpha}\left(\alpha - \alpha_t\right) + C_{D_M}\frac{\overline{V}-\overline{V}_t}{\overline{V}_s} + C_{Df'}\left\langle \eta, \zeta \right\rangle \\
C_L ={}& C_{Lt,c} + C_{L_\alpha}\left(\alpha - \alpha_t\right) + C_{L_M}\frac{\overline{V}-\overline{V}_t}{\overline{V}_s} + \ldots \\
& C_{L_{\dot\alpha}}\dot\alpha + \frac{\bar c}{2\overline{V}_t}C_{L_q}q + C_{L_{\delta_e}}\left(\delta_e - \delta_{et}\right) + C_{Lf'}\left\langle \eta, \zeta \right\rangle \\
C_Y ={}& C_{Y_\beta}\beta + \frac{b}{2\overline{V}_t}C_{Y_p}p + \frac{b}{2\overline{V}_t}C_{Y_r}r + C_{Y_{\delta_a}}\delta_a + \ldots \\
& C_{Y_{\delta_r}}\delta_r + C_{Yf'}\left\langle \eta, \zeta \right\rangle \\
C_l ={}& C_{l_\beta}\beta + \frac{b}{2\overline{V}_t}C_{l_p}p + \frac{b}{2\overline{V}_t}C_{l_r}r + C_{l_{\delta_a}}\delta_a + \ldots \\
& C_{l_{\delta_r}}\delta_r + C_{lf'}\left\langle \eta, \zeta \right\rangle \\
C_m ={}& C_{m_0} + C_{m_\alpha}\alpha + C_{m_{\dot\alpha}}\dot\alpha + C_{m_M}\frac{\overline{V}-\overline{V}_t}{\overline{V}_s} + \ldots \\
& \frac{\bar c}{2\overline{V}_t}C_{m_q}q + C_{m_{\delta_e}}\delta_e + C_{mf'}\left\langle \eta, \zeta \right\rangle \\
C_n ={}& C_{n_\beta}\beta + \frac{b}{2\overline{V}_t}C_{n_p}p + \frac{b}{2\overline{V}_t}C_{n_r}r + C_{n_{\delta_a}}\delta_a + \ldots \\
& C_{n_{\delta_r}}\delta_r + C_{nf'}\left\langle \eta, \zeta \right\rangle
\end{aligned}
\tag{1}
$$

Where, $C_{A_B} \equiv \frac{\partial C_A}{\partial B}$

The aerodynamic and physical parameters for the Boeing-747 were extracted from Heffley and Jewell (1972) for the cruise flight condition ($M = 0.8$, 40000 ft altitude). The interaction coefficients were determined for the Boeing-747 using an approximate model which assumed a symmetrical lift distribution (leading aircraft) with no sweep or dihedral. The approximations are assumed to be acceptable in

developing the control system. Longitudinal separation is fixed at a distance of 10 wingspans. Longitudinal separation variation around this point will have little effect as the vortices stay nearly constant in strength and diameter for small longitudinal changes.

The induced forces and moments are highly non-linear, which creates an interesting control and trim problem. The functions that describe these forces and moments are repeated in (2) and (3) for the convenience of the reader.

The incremental drag and rolling moment coefficients are reproduced in Fig. 1. These plots clearly indicate that the optimum position for drag reduction corresponds to the largest rolling moments. The plots show results which are significant for the trim calculations shown later.
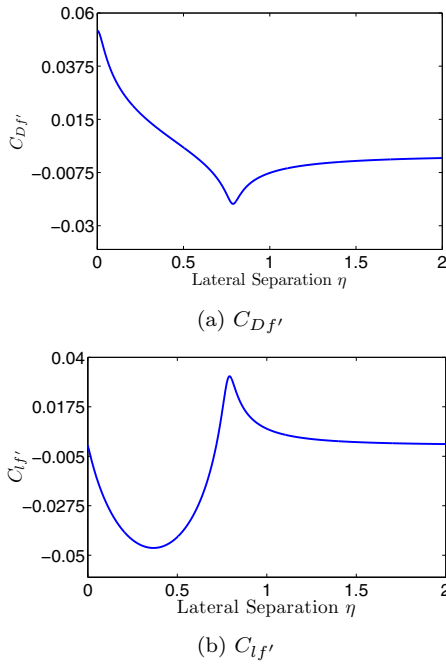

(a) $C_{Df'}$

(b) $C_{lf'}$

Fig. 1. Induced drag and rolling moment coefficient as functions of lateral separation η and vertical separation $\zeta = 0$

$$
\begin{aligned}
C_{Df'} &= \frac{2C_{L,k}C_{L,j}}{\pi^3 AR}\sigma_{jk} \\
C_{Lf'} &= \frac{-c_{l_\alpha}C_{L,j}}{2\pi^2 AR}\sigma_{jk} \\
C_{Yf'} &= \frac{S_f}{S}\frac{2C_{L,j}}{\pi AR\zeta_f}\sigma_{jkf} \\
C_{lf'} &= \frac{c_{l_\alpha}C_{L,j}}{2\pi^2 AR}\tau_{jk} \\
C_{mf'} &= C_{Lf'}(h - h_0) - V_T C_{L\omega_h f'}\left(1 - \frac{d\epsilon}{d\alpha}\right) \\
C_{L\omega_h f'} &= \frac{-2a_1 C_{L,j}}{\pi^3 AR\eta_h}\sigma_{jk\omega_h} \\
C_{nf'} &= \frac{2C_{L,k}C_{L,j}}{\pi^3 AR}\tau_{jk} - V_f\frac{2C_{L,j}}{\pi AR\zeta_f}\sigma_{jkf}
\end{aligned}
\tag{2}
$$

$$
\begin{aligned}
\sigma_{jk} &= \ln\left|\frac{\left((\eta-(\pi/4))^2+\zeta^2+\mu^2\right)\left((\eta+(\pi/4))^2+\zeta^2+\mu^2\right)}{(\eta^2+\zeta^2+\mu^2)^2}\right| \\
\sigma_{jkf} &= \ln\left|\frac{(\eta-\pi/8)^2+(\zeta+\zeta_v)^2+\mu^2}{(\eta-\pi/8)^2+(\zeta+\zeta_v-\zeta_f\pi/8)^2+\mu^2}\right|\dots \\
&\quad - \ln\left|\frac{(\eta+\pi/8)^2+(\zeta+\zeta_v)^2+\mu^2}{(\eta+\pi/8)^2+(\zeta+\zeta_v-\zeta_f\pi/8)^2+\mu^2}\right| \\
&\dots
\end{aligned}
\tag{3}
$$

$$
\begin{aligned}
\tau_{jk} &= -2\sqrt{\zeta^2+\mu^2}\left[\tan^{-1}\left(\frac{\eta-\pi/4}{\sqrt{\zeta^2+\mu^2}}\right)\dots\right. \\
&\quad \left. + \tan^{-1}\left(\frac{\eta+\pi/4}{\sqrt{\zeta^2+\mu^2}}\right) - 2\tan^{-1}\left(\frac{\eta}{\sqrt{\zeta^2+\mu^2}}\right)\right]\dots \\
&\quad -\eta\ln\left|\frac{\left((\eta-\pi/4)^2+\zeta^2+\mu^2\right)\left((\eta+\pi/4)^2+\zeta^2+\mu^2\right)}{(\eta^2+\zeta^2+\mu^2)^2}\right|\dots \\
&\quad -\frac{\pi}{8}\ln\left|\frac{(\eta+\pi/4)^2+\zeta^2+\mu^2}{(\eta-\pi/4)^2+\zeta^2+\mu^2}\right| \\
\sigma_{jk\omega_h} &= \ln\left|\frac{\left(\zeta^2+\left(\eta-\frac{\pi}{8}-\frac{\pi}{8}\eta_h\right)^2+\mu^2\right)\left(\zeta^2+\left(\eta+\frac{\pi}{8}+\frac{\pi}{8}\eta_h\right)^2+\mu^2\right)}{\left(\zeta^2+\left(\eta-\frac{\pi}{8}+\frac{\pi}{8}\eta_h\right)^2+\mu^2\right)\left(\zeta^2+\left(\eta+\frac{\pi}{8}-\frac{\pi}{8}\eta_h\right)^2+\mu^2\right)}\right|
\end{aligned}
$$

The reduction in induced drag through formation flight is achieved by taking advantage of the pair of trailing vortices generated as the lead aircraft produces lift. When positioned outboard of this pair of trailing vortices, a varying upwash is induced along the lifting surfaces of the following aircraft. This causes an increased effective angle of attack which both increases and rotates the resulting aerodynamic forces on the wing and empennage. The resulting increase in lift and reduction of induced drag allow the aircraft to be re-trimmed for improved range performance. At the optimal relative positioning however, the lateral moments and side force experienced require significant control surface deflections for trim which reduces obtainable formation flight benefit (Kless et al. 2012).

The strength of the induced flow is a function of the circulation strength of the trailing vortices and the relative separation of these to position of the trailing aircraft. Depending on the methodology used, the region of optimum lateral separation is predicted anywhere between $b < \eta \leq \pi b/4$, with $\zeta = 0$, and with all methods predicting a very small region of peak drag benefit on the order of 10% of the span (Bower et al. 2009, Blake and Gingras 2004). In a two aircraft formation, this optimum position corresponds to the position of highest induced rolling moments which can be high enough to saturate the ailerons of the trailing aircraft. In order to take full advantage of the formation flight effects, the trailing aircraft must therefore be controlled with a high degree of position accuracy while coping with large rolling moments.

2.2 Trim Actuator Settings

The required trim actuator settings can be calculated over a range of vertical and lateral separations using the aerodynamic equations in (1), along with basic thrust and gravity models.

First, the trim settings for the conventional airliner in isolated flight is calculated. This is done under the assumptions that trim angle of attack α_t and thus the trim pitch angle θ_t are small, and that the lift is much larger than the drag. Equation (4) then shows how the trim angle of attack and elevator settings are solved. Aileron and rudder settings will be kept at 0° deflection.

$$
\begin{bmatrix} \alpha_t \\ \delta_{e_t} \end{bmatrix} = \begin{bmatrix} C_{L_\alpha} & C_{L_{\delta_e}} \\ C_{m_\alpha} & C_{m_{\delta_e}} \end{bmatrix}^{-1} \begin{bmatrix} \frac{mg}{\bar{q}_t S} - C_{L_0} \\ -C_{m_0} \end{bmatrix}
\tag{4}
$$

The trim thrust requirement can then be calculated using (5).

(a) Elevator Deflection

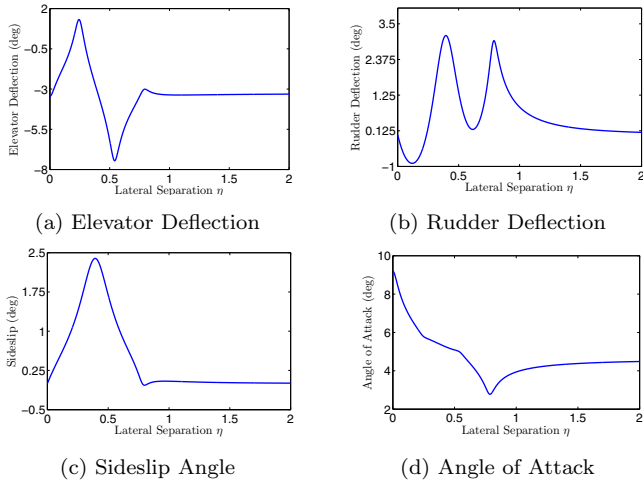(b) Rudder Deflection

(c) Sideslip Angle

(d) Angle of Attack

Fig. 2. Trim settings and states for $\zeta = 0$ (Full required settings for formation flight)

$$T_t = \bar{q}_t S C_{Dt} \cos \alpha_t - \bar{q}_t S C_{Lt} \sin \alpha_t + mg \sin \theta_t \qquad (5)$$

Next, (1) is solved with all forces and moments in trim (i.e. lift force cancels gravity force, side-force and moments all equal 0). The equations for formation flight effect's contribution to the trim settings and states is solved simultaneously. Note that the formation and conventional settings can be superimposed as (1) is a linearised model.

Equation (5) is then used to find the total throttle setting using full trim settings and states. The full, non-linear equation can be used here as it is given in (5).

Fig. 2 shows the resulting required trim settings and states for a vertical separation of zero. The required aileron trim setting is shown with the required trim thrust in Fig. 3. Note that the required aileron trim settings vary between large negative and positive deflections. Such large aileron deflections do not physically make sense. However, it should be noted that a linear model is used, and this is therefore simply an indication to which extent the ailerons are insufficient in certain regions of formation flight. The physical implications are that the rolling moment will overpower the ailerons and the aircraft will be forced into a roll and out of formation flight.

2.3 Trim Ranges

Next, it is necessary to analyse the trim throttle setting function as shown on Fig. 3. By comparing this to the required setting for conventional flight, a range of fuel-consumption benefit is identified with the assumption that a lower throttle setting equates to lower fuel-consumption. It is interesting to note that if the follower aircraft is directly behind the leader aircraft, the formation flight interactions adversely affect overall drag reduction. This is explained by the vortices pushing down on both wings of the follower aircraft, effectively reducing lift without inducing moments.

The airliner is not trimmable at the optimal fuel consumption location due to the fact that the induced rolling moment requires aileron trim deflections which are outside the physical deflection limits.
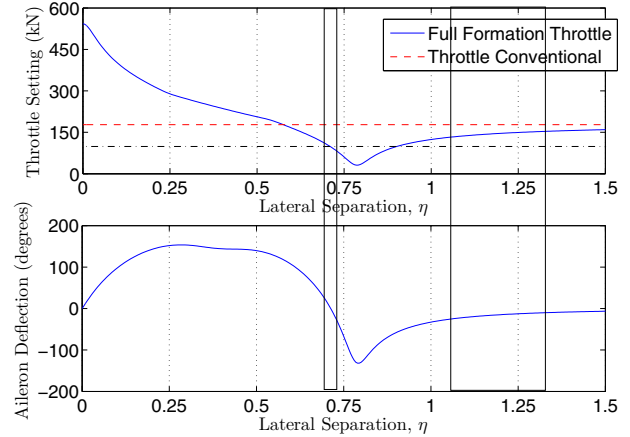

Fig. 3. Comparison of trim regions for $\zeta = 0$, showing trim aileron and throttle settings.

Inspecting Fig. 3, two valid trim regions are found however. The first is a "sandwich" region, which is a narrow region sandwiched between two untrimmable regions. The second is an "outer" region, which only has an untrimmable region on its inside. The rectangle for sandwich region shows a range between maximum aileron settings of $-25°$ to $25°$. The rectangle for the outer region indicates an area between a maximum required aileron deflection of $-25°$, and a chosen trim of $-10°$ aileron deflection.

Each region comes with its own advantages and disadvantages. The sandwich region has a better fuel-consumption reduction due to a lower induced drag at trim. Furthermore, it is possible to have a 0° aileron deflection, which will avoid unmodelled drag effects on the ailerons. The small width of the sandwich region may be impractical for the trailing aircraft to track in real atmospheric conditions. In the sandwich region, the core of the trailing vortex will be impinging on the wing of the trailing aircraft, which will induce large angles of attack. This may invalidate the assumptions of the aerodynamic model. Furthermore, the induced rolling moments at each extreme of this region is in the direction that would naturally roll the aircraft further into the untrimmable region, worsening the problem.

The outer region is a safer option however, as the aircraft does not have to stay in such a narrow following region as for the sandwich region. Furthermore, the induced rolling moment near the outer region is in a direction that will tend to naturally push the aircraft away from the untrimmable region, giving it the potential for inherent fault recovery. However, the outer region will have a non-zero rolling moment, which results in the need for a non-zero aileron deflection which will introduce unmodelled drag. Lastly, it may be a simpler task of initiating formation flight for the outer trim region. It is thus clear that this is a risk versus benefit consideration.

Fig. 4 compares the required aileron and thrust settings over a range of vertical separations for both trim regions. These plots indicate that the best fuel consumption gain for both regions are at zero vertical separation. Furthermore, it is evident that the trim is more sensitive to

(a) Throttle setting comparison
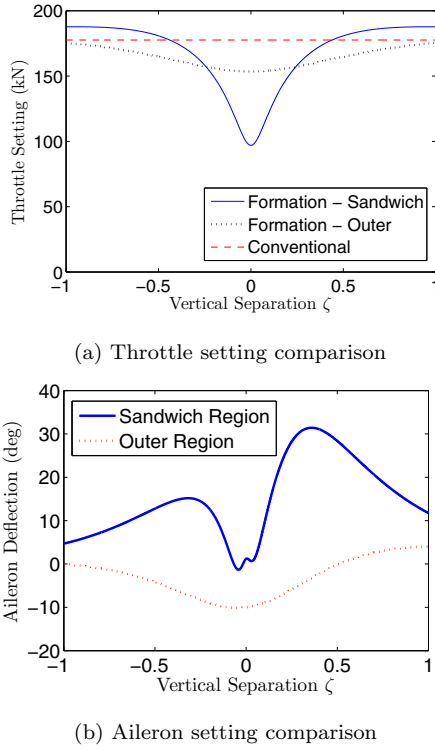

(b) Aileron setting comparison

Fig. 4. Comparison of sandwich ($\eta = 0.713$) and outer ($\eta = 1.33$) region trim settings over vertical displacement

lateral separation changes than it is to vertical separation changes.

3. LINEAR DYNAMICS ANALYSIS

Following the trim analysis, the next step is to derive the linearised dynamic model of the aircraft about each calculated trim as a function of lateral and vertical displacement. An eigenvalue analysis of the linearised model is then performed to observe how the dynamic response of the aircraft changes over the range of lateral and vertical displacements.

3.1 State Space Representation

The conventional dynamic model of an aircraft in isolated flight is traditionally separated into sets of longitudinally and laterally decoupled states. Any coupling present between the states is insignificant enough to be neglected and can be treated as a disturbance during the design of the flight control systems. Equations (6) shows the format of the conventional linearised system.

$$
\begin{aligned}
\dot{\mathbf{x}}_{\text{long}} &= \mathbf{A}_{\text{long}}\mathbf{x}_{\text{long}} + \mathbf{B}_{\text{long}}\mathbf{u}_{\text{long}} \\
\dot{\mathbf{x}}_{\text{lat}} &= \mathbf{A}_{\text{lat}}\mathbf{x}_{\text{lat}} + \mathbf{B}_{\text{lat}}\mathbf{u}_{\text{lat}}
\end{aligned}
\tag{6}
$$

For formation flight, the state vectors are expanded in (7) to include formation flight interaction states η, ζ and $\Delta\psi$, which are the lateral separation, vertical separation, and the difference in the heading angle between the formation leader and follower respectively. $\Delta\psi$ is required for the description of the formation flight differential equations in (8).

$$
\begin{aligned}
\mathbf{x}_{\text{long}} &= \begin{bmatrix} \overline{V} & \alpha & q & \theta & \zeta \end{bmatrix}^T \\
\mathbf{x}_{\text{lat}} &= \begin{bmatrix} \beta & p & r & \phi & \eta & \Delta\psi \end{bmatrix}^T
\end{aligned}
\tag{7}
$$

$$
\begin{aligned}
\dot{\zeta} &= \frac{\overline{V}_t}{b}\sin(\theta - \alpha) \approx \frac{\overline{V}_t}{b}(\theta - \alpha) \\
\dot{\eta} &= \frac{\overline{V}_t}{b}\sin(\Delta\psi) \approx \frac{\overline{V}_t}{b}(\Delta\psi) \\
\dot{\psi} &= q\sin\phi\sec\theta + r\cos\phi\sec\theta
\end{aligned}
\tag{8}
$$

Following initial derivations of the state space representation, it was concluded that significant coupling exists between the lateral and longitudinal subsystems, and a full model was derived. Equation (9) shows the format of this.

$$
\dot{\mathbf{x}}_{\text{full}} = \begin{bmatrix} \mathbf{A}_{\text{long}} & \mathbf{A}_{\text{long-lat}} \\ \mathbf{A}_{\text{lat-long}} & \mathbf{A}_{\text{lat}} \end{bmatrix}\mathbf{x}_{\text{full}} + \mathbf{B}_{\text{full}}\mathbf{u}_{\text{full}}
\tag{9}
$$

Equations (10) - (13) show the sub-matrices. Large terms are indicated as partial derivatives and expanded in (14) - (16). Note that B_{full} was omitted as its derivation is considered trivial and irrelevant to this particular analysis.

$$
\mathbf{A}_{\text{long}} = \begin{bmatrix}
\frac{\partial\dot{\overline{v}}}{\partial\overline{v}} & \frac{\partial\dot{\overline{v}}}{\partial\alpha} & 0 & \frac{\partial\dot{\overline{v}}}{\partial\theta} & \frac{\partial\dot{\overline{v}}}{\partial\zeta} \\
\frac{\partial\dot{\alpha}}{\partial\overline{v}} & \frac{\partial\dot{\alpha}}{\partial\alpha} & \frac{\partial\dot{\alpha}}{\partial q} & \frac{\partial\dot{\alpha}}{\partial\theta} & \frac{\partial\dot{\alpha}}{\partial\zeta} \\
\frac{\partial\dot{q}}{\partial\overline{v}} & \frac{\partial\dot{q}}{\partial\alpha} & \frac{\partial\dot{q}}{\partial q} & 0 & \frac{\partial\dot{q}}{\partial\zeta} \\
0 & 0 & 1 & 0 & 0 \\
0 & -\frac{\overline{V}_t}{b} & 0 & \frac{\overline{V}_t}{b} & 0
\end{bmatrix}
\tag{10}
$$

$$
\mathbf{A}_{\text{lat}} = \begin{bmatrix}
\frac{\partial\dot{\beta}}{\partial\beta} & 0 & -1 & \frac{\partial\dot{\beta}}{\partial\phi} & \frac{\partial\dot{\beta}}{\partial\eta} & 0 \\
\frac{\partial\dot{p}}{\partial\beta} & \frac{\partial\dot{p}}{\partial p} & \frac{\partial\dot{p}}{\partial r} & 0 & \frac{\partial\dot{p}}{\partial\eta} & 0 \\
\frac{\partial\dot{r}}{\partial\beta} & \frac{\partial\dot{r}}{\partial p} & \frac{\partial\dot{r}}{\partial r} & 0 & \frac{\partial\dot{r}}{\partial\eta} & 0 \\
0 & 0 & 1 & \tan\theta_t & 0 & 0 \\
0 & 0 & 0 & 0 & 0 & \frac{\overline{V}_t}{b} \\
0 & 0 & \sec\theta_t & 0 & 0 & 0
\end{bmatrix}
\tag{11}
$$

$$
\mathbf{A}_{\text{long-lat}} = \begin{bmatrix}
0 & 0 & 0 & 0 & \frac{\partial\dot{\overline{v}}}{\partial\eta} & 0 \\
0 & 0 & 0 & 0 & \frac{\partial\dot{\alpha}}{\partial\eta} & 0 \\
0 & 0 & 0 & 0 & \frac{\partial\dot{q}}{\partial\eta} & 0 \\
0 & 0 & 0 & 0 & 0 & 0 \\
0 & 0 & 0 & 0 & 0 & 0
\end{bmatrix}
\tag{12}
$$

$$
\mathbf{A}_{\text{lat-long}} = \begin{bmatrix}
0 & 0 & 0 & 0 & \frac{\partial\dot{\beta}}{\partial\zeta} \\
0 & 0 & 0 & 0 & \frac{\partial\dot{p}}{\partial\zeta} \\
0 & 0 & 0 & 0 & \frac{\partial\dot{r}}{\partial\zeta} \\
0 & 0 & 0 & 0 & 0 \\
0 & 0 & 0 & 0 & 0 \\
0 & 0 & 0 & 0 & 0
\end{bmatrix}
\tag{13}
$$

Longitudinal Elements

$$
\begin{aligned}
\frac{\partial\dot{\overline{v}}}{\partial\overline{v}} &= -\frac{\rho\overline{V}_t S(C_{Dt})}{m} - \frac{\bar{q}_t S}{m}\frac{C_{D_M}}{V_s} \\
\frac{\partial\dot{\overline{v}}}{\partial\alpha} &= -\frac{T}{m}\sin(\alpha_t) - \frac{\bar{q}_t S}{m}C_{D_\alpha} + g \\
\frac{\partial\dot{\overline{v}}}{\partial\theta} &= -g \\
\frac{\partial\dot{\overline{v}}}{\partial\zeta} &= \frac{\bar{q}_t S C_{L,j}}{m\pi^2 AR}\left(\frac{2C_{L,k}}{\pi} + \frac{c_{l\alpha}\alpha_t}{2}\right)\frac{\partial\sigma_{j,k}}{\partial\zeta}\bigg|_t
\end{aligned}
\tag{14}
$$

$\cdots$

$$\frac{\partial \dot{\alpha}}{\partial \overline{v}} = -\frac{\rho S C_{Lt}}{m} - \frac{q_t S C_{L_M}}{\overline{V}_t m V_s}$$

$$\frac{\partial \dot{\alpha}}{\partial \alpha} = -\frac{\bar{q}_t S C_{L_\alpha}}{m \overline{V}_t}$$

$$\frac{\partial \dot{\alpha}}{\partial q} = 1 - \frac{\bar{q}_t S \bar{c} C_{LQ}}{2 \overline{V}_t^2 m}$$

$$\frac{\partial \dot{\alpha}}{\partial \theta} = -\frac{g}{V_t} \sin \theta_t$$

$$\frac{\partial \dot{\alpha}}{\partial \zeta} = \frac{\bar{q}_t S C_{L,j}}{m \overline{V}_t \pi^2 AR} \left(\frac{c_{l_\alpha}}{2} - \frac{2 C_{L,k} \alpha_t}{\pi} \right) \left. \frac{\partial \sigma_{j,k}}{\partial \zeta} \right|_t$$

$$\frac{\partial \dot{q}}{\partial \overline{v}} = \frac{\bar{q}_t S \bar{c} C_{m_M}}{I_{yy} V_s}$$

$$\frac{\partial \dot{q}}{\partial \alpha} = \frac{\bar{q}_t S \bar{c}}{I_{yy}} C_{m_\alpha}$$

$$\frac{\partial \dot{q}}{\partial q} = \frac{\bar{q}_t S \bar{c}^2}{2 I_{yy} \overline{V}_t} C_{m_Q}$$

$$\frac{\partial \dot{q}}{\partial \zeta} = \frac{\bar{q}_t S \bar{c} C_{L,j}}{I_{yy} \pi^2 AR} \left[\frac{-c_{l_\alpha}}{2} \left(\left. \frac{\partial \sigma_{j,k}}{\partial \zeta} \right|_t \right) (h - h_0) + \cdots \right.$$
$$\left. \overline{V}_t \left(1 - \frac{d\epsilon}{d\alpha} \right) \left(\frac{2a_1}{\pi \eta_h} \left. \frac{\partial \sigma_{jkw_h}}{\partial \zeta} \right|_t \right) \right]$$

Lateral Elements

$$\frac{\partial \dot{\beta}}{\partial \beta} = \frac{\bar{q}_t S}{m \overline{V}_t} \left(C_{Y_\beta} + C_{Dt} - C_{Lt} \alpha_t \right)$$

$$\frac{\partial \dot{\beta}}{\partial p} = \frac{\bar{q}_t S b}{2 m \overline{V}_t^2} C_{Y_P}$$

$$\frac{\partial \dot{\beta}}{\partial r} = \frac{\bar{q}_t S}{m \overline{V}_t} C_{Y_R} - 1$$

$$\frac{\partial \dot{\beta}}{\partial \phi} = \frac{g}{V_t} \cos \theta_t$$

$$\frac{\partial \dot{\beta}}{\partial \eta} = \frac{2 S_f \bar{q}_t C_{L,j}}{\overline{V}_t m \pi AR \zeta_f} \left(\left. \frac{\partial \sigma_{jkf}}{\partial \eta} \right|_t \right)$$

$$\frac{\partial \dot{p}}{\partial \beta} = \frac{\bar{q}_t S b}{I_{xx}} C_{l_\beta}$$

$$\frac{\partial \dot{p}}{\partial p} = \frac{\bar{q}_t S b^2}{2 I_{xx} \overline{V}_t} C_{l_P}$$

$$\frac{\partial \dot{p}}{\partial r} = \frac{\bar{q}_t S b^2}{2 I_{xx} \overline{V}_t} C_{l_R}$$

$$\frac{\partial \dot{p}}{\partial \eta} = \frac{\bar{q}_t S b c_{l_\alpha} C_{L,j}}{2 I_{xx} \pi^2 AR} \left(\left. \frac{\delta \tau_{jk}}{\delta \eta} \right|_t \right)$$

$$\frac{\partial \dot{r}}{\partial \beta} = \frac{\bar{q}_t S b}{I_{zz}} C_{n_\beta}$$

$$\frac{\partial \dot{r}}{\partial p} = \frac{\bar{q}_t S b^2}{2 \overline{V}_t I_{zz}} C_{n_P}$$

$$\frac{\partial \dot{r}}{\partial r} = \frac{\bar{q}_t S b^2}{2 \overline{V}_t I_{zz}} C_{n_R}$$

$$\frac{\partial \dot{r}}{\partial \eta} = \frac{2 \bar{q}_t S b C_{L,j}}{I_{zz} \pi AR} \left(\frac{C_{L,k}}{\pi^2} \left. \frac{\partial \tau_{jk}}{\partial \eta} \right|_t - \frac{\overline{V}_f}{\zeta_f} \left. \frac{\partial \sigma_{jkf}}{\partial \eta} \right|_t \right)$$

$$(15)$$

Coupling Elements

$$\frac{\partial \dot{\overline{v}}}{\partial \eta} = \frac{\bar{q}_t S C_{L,j}}{m \pi^2 AR} \left(\frac{2 C_{L,k}}{\pi} + \frac{c_{l_\alpha} \alpha_t}{2} \right) \left. \frac{\partial \sigma_{j,k}}{\partial \eta} \right|_t$$

$$\frac{\partial \dot{\alpha}}{\partial \eta} = \frac{\bar{q}_t S C_{L,j}}{m \overline{V}_t \pi^2 AR} \left(\frac{c_{l_\alpha}}{2} - \frac{2 C_{L,k} \alpha_t}{\pi} \right) \left. \frac{\partial \sigma_{j,k}}{\partial \eta} \right|_t$$

$$\frac{\partial \dot{q}}{\partial \eta} = \frac{\bar{q}_t S \bar{c} C_{L,j}}{I_{yy} \pi^2 AR} \left[\frac{-c_{l_\alpha}}{2} \left(\left. \frac{\partial \sigma_{j,k}}{\partial \eta} \right|_t \right) (h - h_0) + \cdots \right.$$
$$\left. \overline{V}_t \left(1 - \frac{d\epsilon}{d\alpha} \right) \left(\frac{2a_1}{\pi \eta_h} \left. \frac{\partial \sigma_{jkw_h}}{\partial \eta} \right|_t \right) \right]$$

$$\frac{\partial \dot{\beta}}{\partial \zeta} = \frac{2 S_f \bar{q}_t C_{L,j}}{\overline{V}_t m \pi AR \zeta_f} \left(\left. \frac{\partial \sigma_{jkf}}{\partial \zeta} \right|_t \right)$$

$$\frac{\partial \dot{p}}{\partial \zeta} = \frac{\bar{q}_t S b c_{l_\alpha} C_{L,j}}{2 I_{xx} \pi^2 AR} \left(\left. \frac{\delta \tau_{jk}}{\delta \zeta} \right|_t \right)$$

$$\frac{\partial \dot{r}}{\partial \zeta} = \frac{2 \bar{q}_t S b C_{L,j}}{I_{zz} \pi AR} \left(\frac{C_{L,k}}{\pi^2} \left. \frac{\partial \tau_{jk}}{\partial \zeta} \right|_t - \frac{\overline{V}_f}{\zeta_f} \left. \frac{\partial \sigma_{jkf}}{\partial \zeta} \right|_t \right)$$

$$(16)$$

The partial derivatives with respect to η and ζ in (14) - (16) are written in terms of influence factors τ_{jk}, σ_{jk}, σ_{jkf} and $\sigma_{jk\omega_h}$. These influence factors are described in Bizinos and Redelinghuys. Their η and ζ derivatives are not explicitly provided here for the sake of saving space, but can easily be determined by using a package such as Matlab's symbolic toolbox.

This state space representation is partially verified by setting the vertical and horizontal separation to very large values, with the hypothesis that this will simulate conventional, isolated flight. The resulting poles are shown in Table 1. An eigenvector analysis proved that the poles are correct according to the mode that they describe.

Table 1: Conventional flight poles

Phugoid mode	$-0.0019 \pm 0.0706i$
Short-period mode	$-0.3259 \pm 0.9009i$
Dutch roll mode	$-0.0197 \pm 0.906i$
Roll mode	-0.6042
Spiral mode	-0.0109

The conventional flight poles in Table 1 were confirmed to be in the correct order of magnitude through comparisons with external sources including Caughy (2011) and Heffley and Jewell (1972).

A controllability analysis revealed that the system is controllable over its defined operating regions using the derived state space model. Observability has not been checked yet, since the configuration of the sensor suite required for formation flight has not been investigated, and the set of available sensor measurements from which the formation flight states will be estimated has not been defined.

3.2 Eigenvalue Analysis

The state space representation model was then used to find poles for both the discussed trim regions. The result is root loci with respect to lateral and vertical separations. Fig. 5 shows the resulting lateral and vertical root loci, a plot of the movement of the poles or eigenvalues, for both trim regions. An analysis of this, accompanied by an eigenvector analysis indicated that the conventional modes are lost, and instead, new modes overpowering in roll angle and roll rate are found. It is also clear that multiple formation flight modes are unstable – where all the conventional modes were stable. These findings were confirmed by a linear simulation, which indicated strong rolling behaviour and complete barrel rolls.

Considering that the root loci for lateral and vertical separation on Fig. 5 are plotted over comparable separation variations for each trim region individually, it is evident that the dynamics change to a much larger extent for vertical separation variation compared to lateral separation variation. In the outer region, the dynamics stay nearly constant for lateral separation variation, as can be seen on Fig. 5b. Note that the root loci are plotted for lateral and vertical separation variations with ranges of 0.1 wingspans, centred across the outer and sandwich trim regions so that they are comparable.

4. CONCLUSION

It was found that there are challenges with trimming the follower aircraft at certain relative positions in the leader's wake vortices. Specifically, it is not possible for the representative airliner to counter the large induced rolling moments at these following positions, including at the optimum region.

Two trimmable regions were found however: the sandwich region, which gives the greatest fuel consumption reduction benefit, but with more risk and practical challenges, and the outer region, which is less risky and more

(a) Lateral sandwich region locus

(b) Lateral outer region locus

(c) Vertical sandwich region locus
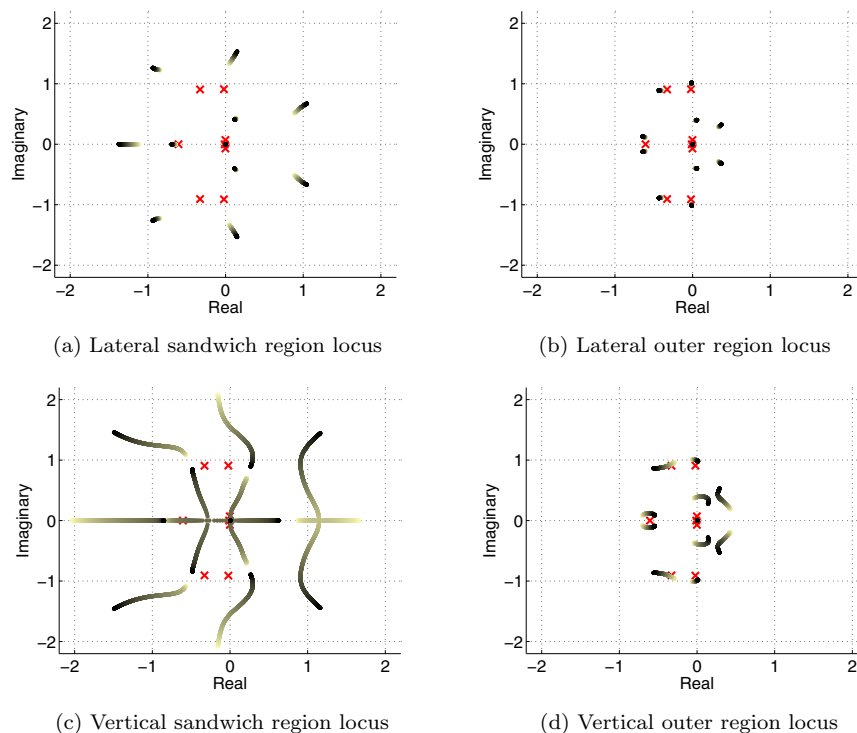
(d) Vertical outer region locus

Fig. 5. Separation loci around trim regions. For vertical separation variation, moving from dark to light indicates upward moving trim changes. For lateral separation variation, moving from dark to light indicates inward moving trim changes. Conventional flight poles are marked with red crosses, and relate to formation flight at infinite separation distances.

practically viable, but with less benefit. Trim and linear dynamics analyses revealed interesting equilibrium and dynamics behaviours for the two regions.

In the sandwich region, the trim changes significantly for lateral separation changes, but less so for vertical separation changes. In the outer region however, the trim is less sensitive to lateral and vertical separation changes. Finally, the dynamics for both regions change significantly for vertical separation variation, but not for lateral separation variation.

Furthermore, the extreme non-linearity of the induced forces and moments present challenges with dynamics changing as a function of spatial separation. These factors indicate that the control system will need to be robust to large changes in the systems characteristics and should be able to disengage the aircraft from formation without endangering the aircraft.

The necessary basis for the design of a formation flight control system has been formed. The next step will be to evaluate a conventional flight controller's performance in a formation flight scenario. Following this, a specialised formation flight controller can be designed.

ACKNOWLEDGEMENTS

REFERENCES

Bizinos, N., Redelinghuys, C. (2012) Tentative study of passenger comfort during formation flight within atmospheric turbulence. *AIAA, Journal of Aircraft.* doi: 10.2514/1.C032018

Blake, W., Gingras D.R. (2004) Comparison of predicted and measured formation flight interference effects. *Journal of Aircraft*, volume 41, pp. 201–207.

Bower, G., Flanzer T., Kroo, I. (2009) Formation geometries and route optimization for commercial formation flight. *AIAA*, paper 2009-3615.

Brodecki, M., Kamesh, S., Qi-Ping, C. (2013a) Formation flight control system for in-flight sweet spot estimation. *AIAA, Aerospace Sciences Meeting including the New Horizons Forum and Aerospace Exposition*, AIAA 2013-1037.

Brodecki, M., Kamesh, S., Qi-Ping, C. (2013b) Emergent behavior of multi-vehicle formations using extremum seeking. *AIAA, Aerospace Sciences Meeting including the New Horizons Forum and Aerospace Exposition*, AIAA 2013-1033.

Caughy, D.A. (2011) Introduction to Aircraft Stability and Control Course Notes for M&AE 5070 *Sibley School of Mechanical & Aerospace Engineering*, Cornell University.

Heffley, R.K., Jewell, W.F. (1972) Aircraft handling qualities data. *NASA*.

Kless, J., Aftosmis, M.J., Ning, S.A., Nemec, M. (2012) Inviscid analysis of extended formation flight. *Seventh International Conference on Computational Fluid Dynamics*

Zou, Y., Pagilla, P.R., Ratliff, R.T. (2009) Distributed formation flight control using constraint forces. *Journal of Guidance, Control and Dynamics*, volume 32, no. 1. doi:10.2514/1.36826